

## Chapter 2

# Introduction to Label-Free Biosensing

This section of the thesis introduces the fundamental concepts related to label-free biosensing and the theoretical concepts related to the resonant photonics employed in this thesis. Starting with an introduction to conventional approaches of molecular detection and medical diagnostics, a range of single-mode label-free biosensing techniques are then presented. The theoretical frameworks that underpin photonic waveguide-based detection strategies are discussed, which then serves to understand and explain the sensing principle of the devices discussed in later chapters. This is followed by an introduction to the most widespread dual-mode sensing principles, namely electrochemical detection combined with optical or acoustic sensing. A presentation of dual-mode electro-photonic silicon biosensing is then given before concluding the chapter with an introduction to functionalisation techniques using self-assembled monolayers.

### 2.1 Motivation

Biosensors that are able to detect disease specific molecular biomarkers play a crucial role across healthcare, from initial diagnosis to optimising and monitoring treatment. Such biosensors need to be able to quantify biological molecules specifically and selectively and with high temporal resolution to accurately monitor their evolution. This combination of requirements can be extremely challenging as a large number of different molecules are present in a clinical sample while only a single one, or a small group of molecules being markers of a specific disease. In addition, it is envisaged that with the introduction of personalised medicine, biomarker profiles rather than individual biomarkers will be required. A highly sensitive, selective and multiplexed biosensing platform is therefore needed to meet all of these requirements [1].

Moreover, many biochemical analytes, including DNA, RNA, proteins, viral capsides, and small molecules are sometimes present at concentration orders of fg/ml

to pg/ml together with other molecules. Biosensor technologies must therefore be highly sensitive.

Detecting biological analytes directly and specifically according to physical properties (such as physical size, mass or charge) is extremely challenging. Most biochemical assays thus exploit the high affinity of a ‘receptor molecule’ towards a specific biomarker. For example, in the case of protein detection, this receptor molecule is typically an antibody raised against the specific protein antigen while a complementary single stranded DNA is used for specific DNA detection. Following binding to the target molecule, the receptor molecule can be functionalised with a ‘label’ that is easy to measure and quantify, for example an enzyme that produces a colorimetric response as in the well established *Enzyme-Linked ImmunoSorbent Assay* (ELISA) [2] technology which enables the detection and quantification of specific antigens in a sample (Fig. 2.1). Particularly, detection at subfemtomolar concentrations has been reported using this assay [3].

The first step in an ELISA assay (Fig. 2.1, 1) is the immobilisation of antibodies at the surface of a well (typically these kind of assays are performed in microwell plates or reaction tubes). The sample containing the complementary antigen is added, leading to the formation of antibody-antigen complexes (Fig. 2.1, 2). Thereafter, the surface is washed with a detergent solution that removes material bound non-specifically to the surface. After this, a second monoclonal antibody which binds to a different region of the target is added (Fig. 2.1, 3). This secondary antibody is modified to carry a reporter enzyme designed to produce a color change when the enzyme reacts with its substrate. If the antigen is present, a complex will have been formed that includes the antibody bound to the well, the antigen and the enzyme-conjugated antibody (Fig. 2.1, 4). To conclude the assay, the specific enzyme substrate is added to produce a visible signal proportional to the quantity of antigen present in the sample (Fig. 2.1, 5).

Even though labels have been essential for implementing nearly all biochemical and cell based assays, this technique presents several practical drawbacks. Firstly,

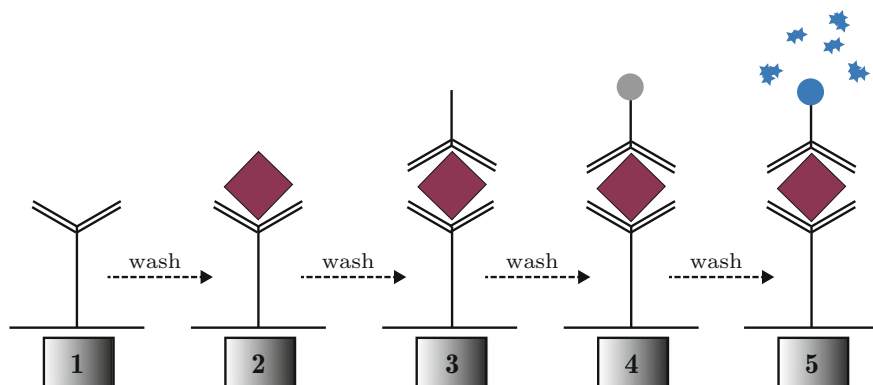


**Fig. 2.1** Followed steps to perform an indirect ELISA assay

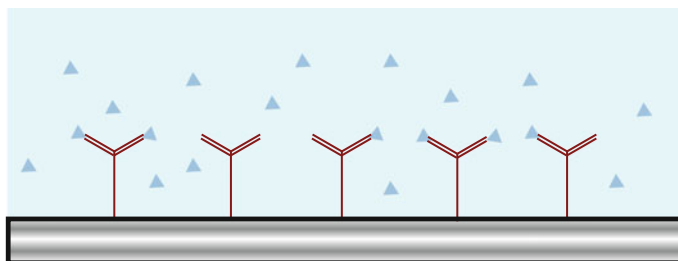


**Fig. 2.2** Example of a label-free sensor transducer. Antibodies (*red*) and antigen (*blue*) are immobilised on the surface of the sensor

labelling assays only provide endpoint read out, and do not allow continuous monitoring. It is thus not possible to provide information on the binding kinetics. Secondly, the multiple washing stages required between each step of the assay often complicates the required sample preparations, reducing the effective throughput and increasing the cost. And finally, the need to identify and produce two different antibodies that recognise different regions of the same target significantly increases the complexity of establishing a reliable assay.

Due to the above considerations, there has been a drive to develop label-free biosensors that reduce assay cost and complexity while providing quantitative information with high throughput. Label-free methods allow to continuously monitor the affinity reaction, providing highly quantitative measures of binding affinity and kinetics [4] and the variation in biomarker concentration over time. Label-free assays are typically surface-based, where the surface of a transducer is functionalised with a layer of receptor molecules. The assay development is also significantly simplified, particularly for highly multiplexed arrays, since only one recognition element is required for each analyte.

The sensor itself consists of a transducer, where the binding event causes a change in a physical property of the sensor which is subsequently measured (Fig. 2.2).

## 2.2 State-of-the-Art Label-Free Technologies

Here I provide a brief overview of some of the most prominent transduction technologies for label-free biosensing applications, while highly relevant publications are also deeply discussed in specific contexts within each chapter of this thesis.

Currently the most widespread and well-known example of label-free biosensor technology is surface plasmon resonance (SPR) [5], which directly measures the local refractive index change induced by biomolecular interactions at a gold surface using surface plasmon waves. Surface plasmons are charge density oscillations that can be excited optically. A number of commercial technologies based on this technique has already been developed by industrial companies such as Biacore (a division of GE

Healthcare), GWC Technologies, IBIS Technologies, Toyobo, GenOptics, SensiQ and Bio-rad. The best limits of detection (typically around  $0.1 \text{ pg/mm}^2$  or  $\text{ng/mL}$  for protein interactions [5–8]) are obtained when interrogating the sensor with angular or wavelength spectroscopy, but then only up to ten measurements can be performed simultaneously [9], limiting the degree of multiplexing and throughput.

With the prospect of providing a robust and practical technology that can deliver limits of detection that rival that of SPR spectroscopy, while still allowing high degree of multiplexing with small fluidic sample consumption and high throughput, multiple technologies have emerged in the last decades.

For instance, sensors based on optical diffraction gratings can measure refractive index changes induced by molecular interactions through a shift of the diffraction wavelength in a fixed direction. They can be mass produced cost-effectively, and also commercial systems for high throughput cell-based assays and drug development are offered by SRU Biosystems and Corning. Nevertheless, simultaneous interrogation of a large number of wells of the microtiter plate in parallel requires optical imaging that only offers end-point read-out [10], instead of the real-time binding curves necessary for analysis of binding kinetics and affinity. Additionally, no highly multiplexed quantitative proteomics at clinically relevant limits of detection has been reported to date.

The potential advantages of integrated photonic sensors have also been exploited in the last decades. They can be easily miniaturised and they offer high potential for chip integration, while showing extremely high sensitivities (pM in a label-free scheme [7, 11, 12]). They also offer a high degree of flexibility in the materials and structures selection, while allowing the fabrication of arrays of sensors with the same characteristics within the same chip for multiplexing analysis. In the case of using silicon photonics technology, they provide additional advantages as are low power consumption and potential for mass production with subsequent reduction of production costs.

Electrochemical label-free techniques (Sect. 2.3.1), such as impedance biosensors and field-effect transistor sensors based on nanowires and carbon nanotubes, are well-suited for highly sensitive integrated systems (for instance, detection of fg/mL concentration values has been reported [13]). However, their performance often deteriorates at physiological ionic strengths (0.15 M), requiring desalting of the sample prior to the measurement [14].

## 2.3 Single-Domain Techniques

A number of strategies have been developed for transducing biomolecular binding between a surface immobilised probe molecule and a target biomarker in solution, including acoustic, electrical or optical sensing principles. Sensing systems which transduce the binding event via a single sensing mechanism can be classified as “single-domain” techniques. This section reviews the most established electrical and

photonic waveguide-based single-domain sensing systems. In-depth reviews of these sensors can be found in [15, 16].

### 2.3.1 *Electronic Biosensing*

A large number of mechanisms can be exploited to transduce a biochemical signal to the electrical domain. Depending on how this transduction is done, a broad subdivision into six classes can be suggested: amperometric/voltammetric biosensors [17], potentiometric biosensors [18], conductometric biosensors [19], impedance biosensors [20] and field-effect transistor (FET) biosensors [21].

Amperometric/voltammetric biosensors measure the change in peak redox current (either oxidation or reduction) of a perturbed capture molecule immobilised on an electrode surface. Here, the capture molecule needs to be an enzyme for which the target is the corresponding enzyme substrate. A notable example is the electrochemical detection of glucose (diabetes biomarker) which employs the enzyme glucose oxidase. Since Clark proposed the first enzyme glucose biosensor in 1962 [22], the field received considerable attention which has led to fast, sensitive (limits of detection down to  $0.18\text{ }\mu\text{M}$  have been reported [23]) and reliable glucose biosensors [24].

Potentiometric biosensors exploit ion-selective electrodes whose potential responds selectively to the concentration of a given ion. Operated under conditions of negligible current flow, this electrode measures the accumulation of charge versus a reference electrode immersed in the analyte solution. In order to apply this principle to biosensing applications, for example the detection of proteins, one has to relate any change in the local concentration of ions at the electrode surface to the binding of the pointed molecules. This technique is capable of operation at extremely low detection limits (below  $\text{ng/mL}$ ) as demonstrated in [25], although in this particular case the high sensitivity is achieved at the expense of throughput (10 h).

Conductance sensors employ a measurement of current flow (i.e. conductance) across a supporting solution that bridges two electrodes. To perform a test using this approach, one needs to link any change in the flow of charge through the substrate (e.g. a nanowire [26]) to the binding of a target to a capture molecule immobilised on the electrode surface. For example, a highly sensitive, conductometric label-free biosensor has been reported based on polyaniline nanowires between gold microelectrodes pairs on silicon [27]. The immobilisation of the immunoglobulin E aptamer onto the engineered nanowire enabled detection of immunoglobulin at concentration as low as  $\text{pg/mL}$  [27].

The most widespread technique employed by the electrochemistry community to sensitively monitor variations on the resistivity/charging capacity of an electrochemical interface is the well-known Electrochemical Impedance Spectroscopy (EIS). This technique employs a small sinusoidal potential superimposed on a DC bias to an electrochemical cell whose impedance is measured as a function of the frequency. The complex impedance, which is defined as  $Z(\omega) = X(\omega) + iY(\omega)$  where  $i$  equal to  $\sqrt{-1}$ , reveals information about the dielectric medium between the electrodes.

$Z(\omega)$  can be modelled as simple equivalent circuit where each component relates to different sections of the dielectric medium as depicted in Fig. 3.15.

When there is a redox related charge transfer across the electrode interface during measurement (Faradaic EIS), published assays employing immobilised surface antibodies are capable of sub ng/mL detection limits for a wide range of targets in aqueous solutions [28–31]. A simpler and potentially more suitable approach for practical applications is found with the absence of this redox probe (non-Faradaic EIS). Employing this technique, M. Dijkema and co-workers [13] were able to detect a biomarker for autoinflammatory and autoimmune disease with a sensitivity of 0.02 fg/mL.

Devices based on field-effect transistors (FETs) have also attracted great attention due to their ability to directly translate the interactions between targeted biological molecules and the FET surface into readable electrical signals [21]. In a standard FET, current flows along a semiconductor path (the channel) that is connected to two electrodes, (the source and the drain). The channel conductance between the source and the drain is switched on and off by a third (gate) electrode that is capacitively coupled through a thin dielectric layer. They can be sufficiently sensitive to achieve protein detection down to pg/mL or even lower levels [32].

Arrays of electrical biosensors have been demonstrated based on some of the detection strategies described previously. These arrays seek to find patient “finger-prints” through the quantification of several tens of markers [33]. For example, simultaneous and real-time detection of three cancer biomarkers has been demonstrated with the use of three antibody modified FET devices with concentrations down to pg/mL [14]. Table 2.1 provides a summary of the different levels of sensitivity obtained by the electrical biosensors discussed in this section.

In contrast to the electrical sensing platform, optical waveguide-based label-free biosensors allow for sophisticated and compact transducers due to the high confinement of light into the waveguide. These optical label-free biosensors evaluate changes in the propagation velocity of electromagnetic fields due to the presence of

**Table 2.1** Summary of the different levels of sensitivity obtained by the electrical biosensors discussed in this section. PB stands for phosphate buffer solution, while PBS for phosphate buffer saline solution. All the sensitivity values reported here were reported without any amplification method

Sensor type	Analyte	Sensitivity	Analyte	Reference
Amperometric	Glucose	32.4 ng/mL	PB	[23, 24]
Potentiometric	Vascular endothelial growth factor	17.35 pg/mL	PB	[25]
Conductance	Immunoglobulin	0.56 pg/mL	PBS	[27]
Non-faradaic EIS	Protein interferon gamma	0.02 fg/mL	PB	[13]
FET	Carcinoembryonic antigen (CEA)	0.5 ng/mL	PBS	[32]

biological particles. They translate changes in the propagation speed of light into a quantifiable signal proportional to the amount of biological material present on the sensor surface.

### 2.3.2 Photonic Waveguide-Based Detection Strategies

Sophisticated and compact label-free biosensors based on optical waveguides exploit the high confinement of light in a waveguide to transduce a biomolecular binding event. Such optical label-free biosensors evaluate changes in the propagation velocity of electromagnetic fields due to the presence of biological particles and translate changes in the propagation speed of light into a quantifiable signal proportional to the amount of biological material present on the sensor surface.

Recently, integrated photonic components based on silicon have become some of the most promising photonic integration platforms. This promise can be attributed to the combination of very high index contrast and the availability of CMOS fabrication technology, which enables the developments and facilities developed for the fabrication of microelectronics to be applied to Photonic Integrated Circuits (PICs) [34]. In this way, it is possible to design and optimise optical label-free biosensors exploiting the most recent progress in the PIC field.

#### 2.3.2.1 Electromagnetic Waves

All the properties of electromagnetic waves, and their interaction with matter, are dictated by the four Maxwell equations [35]. In these equations, light is defined as an electromagnetic wave consisting of sinusoidally-varying electric ( $\mathbf{E}$ ) and magnetic ( $\mathbf{B}$ ) fields. Both fields have the same frequency ( $\nu$ ), are in phase and oscillate perpendicularly to each other. Light then propagates through space on a direction perpendicular to both  $\mathbf{E}$  and  $\mathbf{B}$  and is described by the orientation of the ‘k-vector’ ( $\mathbf{k}$ ), such that  $\mathbf{E}$ ,  $\mathbf{B}$  and  $\mathbf{k}$  are all orthogonal for a plane wave. The ‘wavenumber’ ( $|\mathbf{k}|$ ) can be understood as a spatial angular frequency:  $k = \frac{2\pi}{\lambda}$ , where  $\lambda$  is the wavelength, and the temporal angular frequency being  $\omega = 2\pi\nu$ . Therefore, the Maxwell equations describe the propagation of light in vacuum (where there are no sources or existing electrical charges or currents):

$$\nabla \cdot \mathbf{E} = 0 \quad (2.1)$$

$$\nabla \cdot \mathbf{B} = 0 \quad (2.2)$$

$$\nabla \times \mathbf{E} = -\frac{\partial \mathbf{B}}{\partial t} \quad (2.3)$$

$$\nabla \times \mathbf{B} = \mu_0 \epsilon_0 \frac{\partial \mathbf{E}}{\partial t} \quad (2.4)$$

where  $t$ ,  $\mu_0$  and  $\epsilon_0$  represent the time and the vacuum permeability and permittivity, respectively. For the vacuum case, the two divergence Eqs. (2.1 and 2.2) state that there are no sources or sinks of  $\mathbf{E}$  or  $\mathbf{B}$  fields, while the two curl Eqs. (2.3 and 2.4) indicate that an oscillating magnetic field induces an oscillating electric field, while an oscillating electric field induces an oscillating magnetic field. Thus, due to these inductions between fields, electromagnetic waves do not require a medium in which to propagate. Maxwells equations are coupled first-order partial differential equations, but they can be decoupled to yield separate second-order equations for  $\mathbf{E}$  and  $\mathbf{B}$  [35]:

$$\nabla^2 \mathbf{E} = \mu_0 \epsilon_0 \frac{\partial^2 \mathbf{E}}{\partial t^2} \quad (2.5)$$

$$\nabla^2 \mathbf{B} = \mu_0 \epsilon_0 \frac{\partial^2 \mathbf{B}}{\partial t^2} \quad (2.6)$$

These take the form of equations describing a wave that has a propagation velocity of  $\frac{1}{\sqrt{\mu_0 \epsilon_0}}$ , which equals to speed of light in vacuum ( $c \approx 3 \times 10^8 \text{ms}^{-1}$ ). When an electromagnetic wave passes through a dielectric material, the speed at which light propagates is altered due to the change in the permeability and permittivity of the material ( $\mu$  and  $\epsilon$ , respectively), which is defined as:

$$\frac{1}{\sqrt{\mu\epsilon}} = \frac{c}{n}; n = \sqrt{\frac{\mu\epsilon}{\mu_0\epsilon_0}} \quad (2.7)$$

being  $n$  the refractive index of the material, which represents how the propagation velocity is reduced compared to the vacuum velocity  $c$ . When the electromagnetic wave faces an interface with a material of different  $\epsilon$ , the boundary conditions imposed by Maxwell's equations give rise to Snell's law of refraction and the Fresnel equations, which predict the reflection behaviour of light at a dielectric interface. Moreover, the time-space dependency in Maxwell's equations can be separated due to their linearity. Furthermore, by considering monochromatic harmonic waves (waves with a single frequency  $\omega$ ), they can be solved as:

$$\mathbf{E}(\mathbf{r}, t) = \mathbf{E}(\mathbf{r})e^{-i\omega t} \quad (2.8)$$

$$\mathbf{B}(\mathbf{r}, t) = \mathbf{B}(\mathbf{r})e^{-i\omega t} \quad (2.9)$$

The conformation of the spatial profile  $\mathbf{E}(\mathbf{r})$  depends on the spatial distribution of  $\epsilon$ , and the knowledge of this allows the spatial mode profiles (mode distribution) to be calculated by treating Maxwells equations as an eigenvalue problem. Following



this approach, the resulting mode profiles are the eigenfunctions of the system, while the frequencies ( $\omega$ ) of the modes are the corresponding eigenvalues.

### 2.3.2.2 Silicon Waveguides

A waveguide is a structure that guides the propagation of waves, such as electromagnetic waves or sound waves. In this work, a waveguide guides light over the chip by total internal reflection (from Snell's law of refraction). It is based on a high refractive index core ( $n_2$  in Fig. 2.3) surrounded by a low refractive index cladding ( $n_1$  and  $n_3$  in Fig. 2.3). Here, the high refractive index core is made of silicon while the cladding comprises both air and silicon dioxide.

The waveguide can guide multiple optical modes depending on whether the major electric field component is along the transverse direction (transverse electric modes, quasi-TE modes), or the major magnetic field component is along the transverse direction (transverse magnetic modes, quasi-TM modes) [36]. Each mode propagates across the waveguide with a phase velocity  $\frac{c}{n_{eff}}$ , where  $n_{eff}$  the effective refractive index perceived by the mode. As long as the effective refractive index is larger than the largest refractive index of the cladding (1.44 at 1.55  $\mu\text{m}$  for silicon dioxide ( $\text{SiO}_2$ )), the mode is guided and confined in the waveguide. The higher the effective refractive index, the stronger the confinement.

Power can be transferred between multiple guided modes as light propagates through the waveguide, causing undesired interference effects that distort the transmission spectrum of optical components. To avoid such power transfer, waveguides need to be made sufficiently narrow to limit the number of modes [36]; typically, we use waveguides that only support a single-mode for each polarisation. If the difference between the effective refractive index of the two remaining quasi-TE and quasi-TM modes is large, coupling between these modes will be limited because of the phase mismatch and very different mode profiles. For widths under 520 nm, the silicon photonic waveguide studied here will be single-mode for each polarisation [36].

The dimensions of these waveguides (typically around  $500 \times 220$  nm) at the wavelength of 1.55  $\mu\text{m}$  support the propagation of the quasi-TE mode (Fig. 2.4), which enables very compact and high-performance sensors as a result of this high confinement.

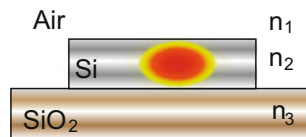
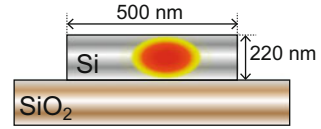


**Fig. 2.3** Cross section profile of a waveguide on a substrate with air cladding. A high-refractive-index core ( $n_2$ ) is surrounded by low-refractive-index media ( $n_1$  and  $n_3$ ) to confine the optical mode

**Fig. 2.4** Illustration of the high mode confinement in a standard waveguide for TE polarised light



Due to the fact that the propagation constant ( $n_{eff}$ ) of an optical mode is obtained together with the mode profile as a solution of the Maxwells equations to the material system via an eigenvalue equation (Sect. 2.3.2.1), it is then conceived that this  $n_{eff}$  will change when the conditions at the waveguide are modified (as occurred when molecules bind to the surface of a waveguide). Perturbation theory states that a change in  $\epsilon(\mathbf{r})$  leads to a change in the propagation constant relative to the size of the fields at the perturbation. Therefore, given that the fields at these perturbations exponentially decrease away from the core of the waveguide, these evanescent tails of the modes effectively sense the action close to the waveguide. This is, for most waveguide systems, a distance of the order  $0.1 - 1 \mu\text{m}$ , and is known as the ‘penetration depth’. This sensing phenomenon is called ‘evanescence wave sensing’, and can be evaluated by any of the waveguiding optical properties (polarisation, intensity, phase, resonance...). In Sect. 2.3.2.5, this sensing mechanism will be discussed in-depth for the sensors employed throughout this thesis.

Another important factor to consider is the waveguide dispersion. Dispersion means that the effective refractive index of a waveguide is strongly dependent on the wavelength. In ring resonator sensors, dispersion plays an important part as we will discuss. The group refractive index of an optical mode is a useful parameter as it takes first-order dispersion into account:

$$n_g = n_{eff} - \lambda \frac{dn_{eff}}{d\lambda} \quad (2.10)$$

with  $n_{eff}$  the effective refractive index and  $\lambda$  the wavelength in vacuum.

Here, all optical modes have a normal first-order dispersion, with a group refractive index that is larger than the effective refractive index. In particular, the group refractive index ( $n_g = 4.35$ ) of the a quasi-TE mode waveguide, as used here, is nearly twice the effective refractive index ( $n_{eff} = 2.33$ ), highlighting the importance of the dispersion.

### 2.3.2.3 Integrated Optical Label-Free Biosensors

Optical waveguides are able to transduce binding events (biochemical signals) into the optical regime; interferometric waveguide sensors (such as Mach-Zehnder interferometers [37] and bi-modal waveguide sensors [38]), photonic crystals (PhC) [39], slot-waveguides [40–42] and ring resonators [43] are examples of this capability. Initially, biosensing performed with integrated optical devices was mainly carried out on Silicon-On-Insulator (SOI) substrates. However, due to the strong water absorption at the operating wavelength of this silicon devices (which limits the performance of

the sensing devices), integrated optical biosensing is nowadays primarily performed on silicon nitride based devices. Here I present a brief review of the biosensing performed with the most widespread and commonly employed devices, while I refer to [11, 12] for very comprehensive reviews of integrated optical label-free biosensors.

Mach-Zehnder interferometers (MZI) utilise the interference between two light-waves of equal wavelength where one of them has experienced a phase delay. Depending on the amount of phase delay (induced by the refractive index medium or optical path length), the optical waves will interfere constructively or destructively. Therefore, functionalising just one of these optical paths, binding events will change the refractive index locally and will induce a shift in the transmission spectrum. MZI have been shown to be able to detect refractive index changes of  $10^{-7}$  RIU [37] and concentrations down to 1 fmol/ $\mu$ L using a silicon nitride substrate [44], while their use for the implementation of labonchip platforms has also been reported [45].

Contrary to MZI, bimodal waveguide interferometry sensors employ a single waveguide to perform the transduction of chemical events. In these sensors, two areas within the waveguide are employed: one operating in a single-mode regime, and a second one that supports two modes (zero- and first-order modes). As the evanescence field has a different distribution for each of the areas, they propagate at different velocities depending on the refractive index of the overlayer. In this way, the interference pattern at the exit of the waveguide changes if the refractive index varies, for instance, as a consequence of a biointeraction event. With this simple approach, based on a silicon nitride substrate, refractive index changes of  $10^{-7}$  RIU [38] and concentrations down to 30 pg/mL of human growth hormone (HGH) [12] have been reported.

PhCs are basically structures with a periodic arrangement of material of different dielectric constant. The periodicity of the structure is very important as it defines the wavelengths that it can support. This periodicity can occur in 1D, 2D or 3D, yet we will discuss 2D structures which are the most widespread configurations. 2D structures have a varying dielectric function in two directions. Typically, triangular or square lattice of air holes are created in semiconductor materials such as silicon. When waves move through such periodic structures they scatter and interfere with themselves. When interference occurs, it results in the diffraction of the wave, forcing it to be sent out of the structure. When interference does not occur (waves that are physically supported by the periodic structure), waves continue to propagate through the structure. In such structures, light can be confined to high quality factor (Q-factor) cavities, directed, split and even slowed down. Their transmission spectrum contains a photonic bandgap in which almost all of the light is reflected for a wavelength range determined by the period of the lattice. Hence, they can be thought of as very efficient wavelength dependent mirrors, with frequencies within the bandgap being strongly reflected. Four detection strategies are used for the detection of biomarkers using PhCs: band-edge detection [46], defect based devices [47], resonant gratings [48] and angular spectrum sensing [49].

As an example of the high sensitivity detection which these devices can achieve, a defect-based PhC can detect 2.5 fg/mL of Bovine Serum Albumin (BSA) [50]. PhC can also be used for a wide range of interesting biosensing applications. For example,

they can be placed on a fiber facet for in-situ sensing [51], used as a sensing device in an imaging method for detection of cancer cell cytotoxicity and proliferation [52] or for resonant surface imaging with high spatial resolution [53]. In the literature, we can find examples of optical biosensor arrays based on PhCs. A method to create large-scale chip-integrated photonic crystal biosensor arrays is demonstrated in [54]. In this example, four defect microcavities are able to sense binding events with 3.35 pg/mL concentrations.

Slot-waveguide sensors consist of two slabs of high refractive index substrates distanced by a nanometer-scale low refractive index slot region and surrounded by low refractive index cladding materials in such a way that light is strongly confined in the slot region. Due to this strong confinement, a stronger light-matter interaction can be achieved within this region as compared to conventional rib or planar waveguides, which results in an enhanced bulk sensitivity. Different slot-waveguide structures have been developed with different structures such as ring resonators [42], photonic crystals [41] and microdisk resonators [40]. However, despite the enhanced light-matter interaction, moderate sensitivity have been reported (changes of  $10^{-6}$  RIU [41] and detection of 30 ng/mL [40]) due to the experimental noise of these systems which limits their sensitivity.

In summary, MZIs present very high sensitivity, however they require large footprints which is limiting for the fabrication of highly dense multiplexed arrays of sensors. PhCs also exhibit extremely high sensitivities due to the strong localisation of the light mode, nevertheless they are very sensitive to fabrication deviations. On the other hand, ring resonator based biosensors have also been extensively examined and also used in commercial products [55], which are more tolerant to fabrication deviations than MZIs and PhCs while still showing high quality resonant factors. This resonant structure, frequently used in integrated photonics, will support our work and is presented in the next section. Finally, a comparison between the different sensitivity levels obtained with the optical sensing techniques presented in this section is given in Table 2.2.

**Table 2.2** Summary of the different levels of sensitivity obtained by the optical biosensors discussed in this section

Sensor type	Analyte	Limit of detection (RIU)	Sensitivity	Reference
MZI	DAPK gene	$10^{-7}$	$\approx 1$ pg/mL	[44]
Bi-modal waveguide	HGH	$10^{-7}$	30 pg/mL	[38]
PhC	BSA	$10^{-5}$	12.5 fg/mL	[50]
PhC array	Avidin	$10^{-4}$	3.35 pg/mL	[54]
Slot-waveguide $\mu$ disk	Streptavidin	$10^{-6}$	30 ng/mL	[40]
Slot-waveguide PhC	Streptavidin	$10^{-6}$	15 ng/mL	[41]

### 2.3.2.4 SOI Ring Resonator Biosensors

Biosensors based on photonic ring resonators have been extensively examined and used in commercial products such as Genalyte [55]. Due to the fact that this resonant structure is robust to fabrication deviations and exhibit high quality resonant factors, it will be used extensively throughout this thesis.

In general, a ring resonator consists of a ring-waveguide and a coupling mechanism to access the loop. A mode propagating through the loop constructively interferes with itself when its wavelength fits an integer number of times in the loop. In other words, the cavity is in resonance when waves that travel in the loop have a round trip phase shift which equals an integer time  $2\pi$ . Thus, the ring is in resonance at wavelengths  $\lambda_{res}$ :

$$\lambda_{res} = \frac{n_{eff}L}{m}, m \in \mathbb{N} \quad (2.11)$$

Here,  $n_{eff}$  is the effective refractive index of the resonant mode and  $L$  is the physical round trip length of the ring resonator. To provide access to its resonance modes, one or more access waveguide are placed next to the ring cavity. Depending on the number of these access waveguides, the whole configuration is called all-pass ring resonator (one access waveguide) or add-drop ring resonator (two access waveguides).

An all-pass ring resonator is a ring resonator in which a fraction  $k$  of the field that is propagating through its access waveguide is coupled into the cavity loop (Fig. 2.5). Without considering losses, the amplitude of this coupled wave is related to the coefficient  $r = \sqrt{1 - k^2}$  [56].

The basic spectral properties of an all-pass ring resonator can be derived by assuming continuous wave regime and matching fields [56]. Assuming that reflections are negligible,  $L$  the physical round trip length of the ring cavity,  $a$  the single-pass amplitude transmission (including propagation losses in both the ring and in the couplers), it is possible to obtain the power transmission from squaring the ratio of the transmitted electrical field and the incident electrical field in the continuous wave regime:

**Fig. 2.5** All-pass ring configuration

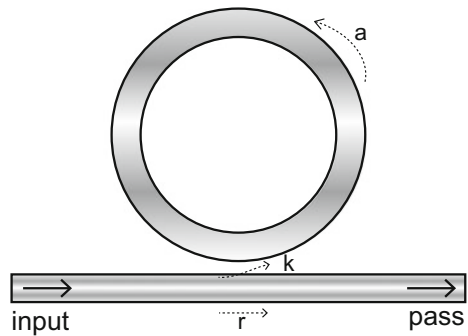
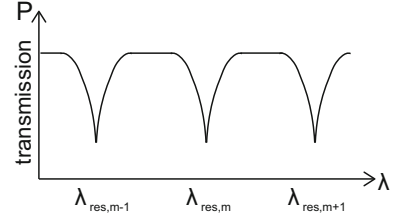


**Fig. 2.6** Transmission spectrum of an all-pass ring resonator, showing dips at the resonance wavelengths



$$T_{allpass}(\lambda) = \frac{I_{pass}}{I_{input}} = \frac{a^2 - 2ar \cos(\frac{2\pi}{\lambda} n_{eff}(\lambda)L) + r^2}{1 - 2ar \cos(\frac{2\pi}{\lambda} n_{eff}(\lambda)L) + (ar)^2} \quad (2.12)$$

Under the assumption of a lossless ring ( $a = 1$ ), the power transmission is unity for all wavelengths, hence the name *all-pass* ring resonator. However, in a practical case, where  $a < 1$ , thus the transmitted power presents minimum values at the resonance wavelengths (Fig. 2.6), due to destructive interference between the access wavelength mode and light coupled back into the waveguide from the ring.

Considering the relation between  $r$  and  $a$ , it can be seen that the ring can be overcoupled ( $r < a$ ), undercoupled ( $r > a$ ) or critically coupled ( $r = a$ ). Critical coupling is an interesting regime for sensing as it allows accurate measurements of the resonance wavelength due to the sharpness that the resonance dip exhibits at this regime [56].

The coupling section, together with the access waveguide and the cavity make up the entire ring resonator. The access waveguide is brought close to the cavity so that the waveguide modes are coupled and power can be transferred from one to another [56]. This coupling is possible due to the portion of the electrical field (associated with the optical mode) that propagates outside the waveguide (commonly called evanescence field). When both waveguides are brought sufficiently close, the evanescence field can couple from the access waveguide into the cavity's waveguide (and vice-versa). Commonly, a directional coupler is employed to couple light from the ring's access waveguide to the ring's cavity and vice-versa.

As Fig. 2.7 shows, the directional coupler employed in the rings of our work consist of a section where two waveguides are close to each other with a gap  $G_c$  over a length  $L_c$ . The power which is transferred can be calculated as [57]:

$$k^2 = \frac{P_{out}}{P_{in}} = \sin^2(\kappa \cdot L_c + \kappa_0) \quad (2.13)$$

**Fig. 2.7** Directional coupler scheme

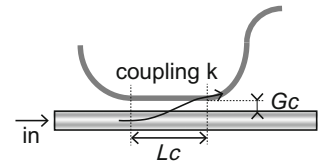
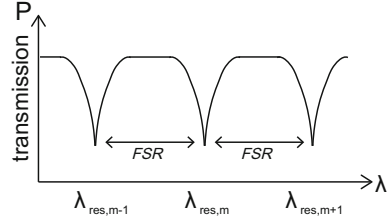


**Fig. 2.8** Power transmission to the drop port of an all-pass ring resonator, where  $FSR$  indicates the spectral distance between subsequent resonances



where  $\kappa [1/\mu m]$  is the coupling coefficient per unit distance in the closest section of the coupler and  $\kappa_0$  is the offset coupling in this region. It is interesting to point out that the coupling strength (both  $\kappa$  and  $\kappa_0$ ) increases with the wavelength, due to a decreasing mode confinement.

A key parameter for the all-pass configuration is the free spectral range (FSR). The FSR represents the spectral distance between subsequent resonances (Fig. 2.8), which as a function of wavelength equals:

$$FSR = \frac{\lambda^2}{n_g L} \quad (2.14)$$

where  $\lambda$  is the wavelength in vacuum,  $n_g$  is the group refractive index and  $L$  the physical round trip length of the ring's cavity. The transmission spectrum at the drop port of an all-pass ring resonator is depicted in Fig. 2.8, where the FSR is illustrated.

In photonic ring resonator biosensors, a larger FSR in comparison to the estimated  $\Delta\lambda_{resonance}$  is desired in order to be able to accurately monitor the resonance wavelength along an experiment (i.e.  $FSR > \Delta\lambda_{resonance}$ ). In this way, interferences between adjacent resonances originated from large  $\Delta\lambda_{resonance}$  are avoided when monitoring the resonance wavelength.

The performance of ring resonator sensors is mainly limited by losses [56]. Losses have a strong impact on the sharpness of the resonance leading to a reduced accuracy of the peak resonance position, due to the broadening of the resonance dip. Scattering due to sidewall roughness and absorption by the cladding layer are the major loss factors ( $\approx 3$  dB/cm for air cladding and  $\approx 4.7$  dB/cm for water cladding [56]). Moreover, as has been mentioned, bend losses ( $\approx 0.04$  dB/bend) also play an important role in ring resonator performance [56].

### 2.3.2.5 Evanescent Field Sensing with SOI Ring Resonators Biosensors

Biosensors based on ring resonators directly measure selective affinity interactions between analyte molecules in solution and receptor molecules immobilised on the ring waveguide surface (Fig. 2.9).

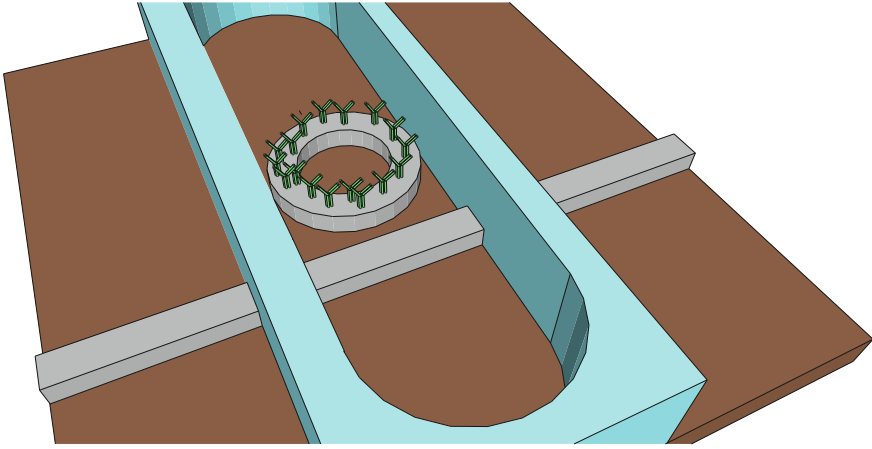
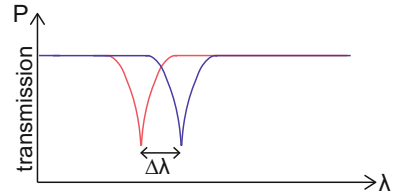


**Fig. 2.9** Ring resonator biosensor coated with immobilised receptor molecules

**Fig. 2.10** Spectral shift of a ring resonator biosensor due to a change in the effective refractive index



Since nearly all biological molecules have a larger refractive index than the surrounding aqueous solvent (for instance,  $n_{\text{antibodies}} \approx 1.45$  Refractive Index Unit (RIU) and  $n_{\text{water}} \approx 1.31$  RIU), this molecular binding increases the local refractive index in the area where the tail of the evanescent field of the waveguide mode is present. The consequent phase change of the waveguide mode produces a measurable shift of the resonance wavelength ( $\Delta\lambda$ ) of the ring (Fig. 2.10). This shift can be monitored to give detailed information about the analyte concentration, affinity between the molecules and the kinetics of the biochemical reaction [57].

The evanescent field of a guided mode is the fraction of the mode that extends in the cladding (out of the waveguide). It decays exponentially with the distance from the core cladding interface [58]:

$$|\vec{E}(d)| = |\vec{E}(0)| \cdot \exp(-\gamma d) \quad (2.15)$$

where  $|\vec{E}(d)|$  is the electric field in the cladding as a function of the distance  $d$  from the interface.  $\gamma$  is the decay constant that is formulated as [59]:

$$\gamma = \frac{2\pi}{\lambda} \sqrt{n_{\text{eff}}^2 - n_w^2} \quad (2.16)$$



Here,  $n_{eff}$  is the effective refractive index of the waveguide mode and  $n_w$  the refractive index of the cladding. Thus, a large refractive index contrast results in a short decay length. This is advantageous when sensing the presence of a thin layer of biomolecules as the mode only will interact with changes in the cladding that happen a few nanometers from the waveguide's surface in the region where the biomolecules are immobilised. In this way, the sensor is very sensitive towards refractive index changes caused by molecular binding near that surface. The greater the overlap between the immobilised molecular layer and the evanescent tail, the more sensitive the sensor. Furthermore, as the sensing zone remains very close to the waveguide's surface, the measurement will be less disturbed by the solution away the surface (improving signal-to-noise ratio). The length of the evanescent tail in solution can be tuned by modifying the geometry of the sensor. This will be exploited in Chap. 6 to quantify conformational changes of immobilised molecules on the surface.

If the refractive index of the cladding changes, the effective refractive index of the waveguide mode will also change (in the range of the waveguide mode evanescent field). Then, the resonance wavelength of the ring resonator mode will shift following the expression [43]:

$$\Delta\lambda_{resonance} = \frac{\lambda_{resonance} \cdot \Delta n_{eff}}{n_g} \quad (2.17)$$

where  $n_g$  is the group index that takes into account the large first order dispersion of the waveguide (Eq. 2.10).

Therefore, the sensitivity for ring resonators is defined as the shift of the resonance wavelength for a certain excitation. For sensing the refractive index of the fluid flowing over the sensor's surface, bulk sensitivity is a more useful metric. Its units are [nm (resonance shift)/RIU]. Another useful metric for evanescence field sensing is the surface sensitivity, which corresponds to the sensitivity of the device upon surface-related molecular interactions. This metric, usually given in [nm (resonance shift)/nm (layer thickness)], provides a quantification of the molecular mass bound to the sensor surface and can help to compare non-optical different technologies with optical ones.

Another important concept related to the sensor's sensitivity is the smallest wavelength shift that can be measured,  $\Delta\lambda_{min}$ , which is associated with the precision of the measurement equipment and the sharpness of the resonance wavelength relative to its central frequency, the quality factor (Q-factor).

Combining these two concepts, it is possible to define the limit of detection (LOD) of a sensor. The LOD refers to the minimum detectable concentration of an analyte in a test sample, and follows:

$$LOD = \frac{\Delta\lambda_{min}}{sensitivity} \quad (2.18)$$

The high Q-factor associated with ring resonators, can result in biosensors with sensitivities comparable to SPR [60]. Detection limits on surfaces of 1.5 pg/mm<sup>2</sup> (corresponding to  $7.6 \times 10^{-7}$  RIU) have been reported with a multiplexed sensing

scheme [61], while cortisol-bovine serum albumin binding has been detected at protein concentrations in solution down to 1 ng/mL [62]. In a more sophisticated example, C. F. Carlborg et al. presented a fully packaged optical device based on slot-waveguide ring resonators sensors [63]. This example employed a variety of ring resonators where the optical signal is confined within two Si waveguides, hence sensing the analyte with the bulk optical signal and not with the evanescence tail. Here, a detection limit of 0.9 pg/mm<sup>2</sup> was demonstrated.

## 2.4 Bi-Domain Techniques

While single-domain techniques have been demonstrated to provide accurate, fast and reliable analysis of chemical events at the surface of the sensor, techniques that monitor these chemical events in two measurement domains can provide further insight into the undergoing molecular and (bio)molecular processes. For this reason, they are readily becoming more popular within the scientific community. For example, dual-mode (or bi-domain) techniques can simultaneously probe both the electrochemical and optical properties of thin films on the surface at the nanometer scale [64], or the viscoelastic properties and conformational state of deposited macromolecules [65]. The number of solutions developed to date for dual-mode (or multi-mode) sensing is significantly more limited than that available for single-domain techniques. Here we highlight the major dual-mode sensing strategies and some of their most relevant applications, while a comparison between them and the system proposed in this thesis is given in Sect. 4.8.

### 2.4.1 *Electrochemical Surface Plasmon Resonance*

SPR has significantly evolved since it was first applied for sensing three decades ago. A range of sub-techniques have also emerged from this sensing technique, including Localised Surface Plasmon Resonance (LSPR) [66], Long-Range Surface Plasmon Resonance (LR-SPR) [67] or Metal-Clad WaveGuide (MCWG) [68], which have been proven to be suitable for performing sensing and imaging. Of particular importance here is the simultaneous characterisation of the optical and electrochemical properties of immobilised molecules on the surface achieved with electrochemical-SPR (EC-SPR). For example, using EC-SPR, characterization of electrochemical DNA sensors has been reported [69], capable of detection of concentrations down to 20 nM. As discussed in Sect. 2.1, SPR sensors directly measure the local refractive index change induced by biomolecular interactions on a gold surface using surface plasmon waves. The transducer translates chemical changes into changes in refractive index, which may be determined by optically interrogating the SPR. The sensor sensitivity, stability, and resolution depend upon properties of both the optical system and the transducing medium. SPR allows the incorporation of a secondary sensing

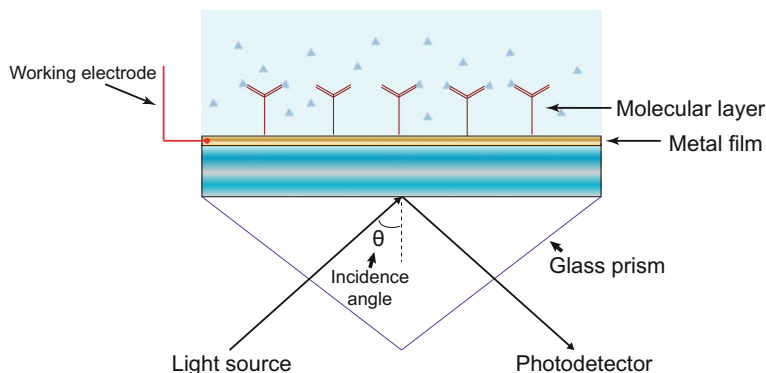


**Fig. 2.11** Electrochemical-SPR schematic diagram with a three electrode cell set-up. The gold substrate that carries the optical surface mode is simultaneously used as the working electrode, allowing simultaneous optical and electrochemical interrogation

domain, here the electrochemical, where the gold substrate that carries the optical surface mode is simultaneously used as the working electrode in a standard three-electrode electrochemical system (Fig. 2.11).

This combination of electrochemical and optical sensing modes can provide deeper insight into redox active system, for example enzymatic reactions [64]. Nevertheless, the EC-SPR technique presents some disadvantages. Firstly, SPR requires a stable optical setup requiring bulky equipment to perform accurate and repeatable measurements. As a consequence, this technique is not a compact solution and thus limits application in point-of-care devices which can be used at the bedside. Secondly, high density arrays of SPR sensors are particularly difficult to engineer.

### 2.4.2 *Electrochemical Quartz Crystal Microbalance with Dissipation Monitoring*

A rapidly emerging label-free biosensor that enables picomolar level detection alongside simultaneous measurements of conformational changes in real-time is Quartz Crystal Microbalance with Dissipation monitoring (QCM-D).

QCM-D relies on a voltage being applied to a piezo electric quartz crystal causing it to oscillate at a specific resonant frequency (Fig. 2.12a). Changes in mass on the quartz surface, for example due to protein binding, result in a change of the resonant frequency of the oscillating crystal. The Sauerbrey relationship (method for correlating changes in the oscillation frequency of a piezoelectric crystal with the mass deposited on it) defines the relationship between mass and resonant frequency for rigid, homogeneous and thin adsorbed layers; the model is not valid for soft or viscoelastic films. In addition to measuring changes in resonant frequency, QCM-D

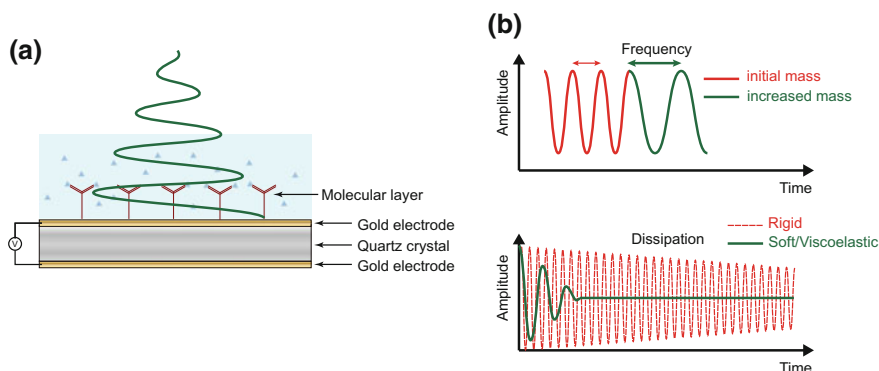


**Fig. 2.12** Electrochemical Quartz crystal Microbalance with Dissipation monitoring (E-QCM-D). **a** The sensor crystal can be coated with a conductive metal layer, which is simultaneously used as the working electrode, allowing simultaneous mechanical and electrochemical interrogation. **b** Both the resonant frequency and the energy dissipation are measured simultaneously for a non-driven sensor crystal

also measures the energy dissipated by the acoustic wave [65]. This is achieved by disconnecting the drive voltage from the crystal while recording the time taken for the oscillation to decay due to damping (Fig. 2.12b). In this system, electrochemical control over the surface of the sensor can also be achieved by coating the quartz sensor with a thin metal layer which acts as the working electrode in a standard three-electrode electrochemical system.

Changes in adsorbed mass of, for example, a rigid protein provide a change in frequency, however for viscoelastic masses such as biomacromolecules, there is also a corresponding change in dissipation, leading to a rapid oscillatory decay of the stored energy in the crystal (Fig. 2.12b). This change in dissipation provides information regarding the viscoelastic properties of the immobilised layer and can thus be used to probe molecular conformation.

Additionally, QCMD allows simultaneous measurements of frequency shift and energy dissipation of multiple different overtones of the fundamental resonance. As higher overtones are more confined into the quartz crystal, while lower overtones are less confined and penetrate further into the supporting analyte, it is possible to also probe the distribution of mass and viscoelasticity as a function of distance into the immobilised layer.

E-QCM-D is an ideal technique for detection of mass on surfaces, as any change in mass on the sensor surface is directly translated onto the resonant frequency. In contrast with optical techniques, E-QCM-D is sensitive to water associated with adsorbed proteins, allowing the quantification of hydrodynamically coupled water (proteins and/or water trapped in cavities in the film).

This electro-mechanical system is also well suited for the detection of enzymatic activities. For instance, a 21 pM threshold of enzymatic activity has been reported while being able to distinguish different hydrolysis mechanisms [70].

### 2.4.3 *Electrochemical Optical Waveguide Lightmode Spectroscopy*

Another (however less developed) optical dual-mode experimental technique has been developed called Electrochemical Optical Waveguide Lightmode Spectroscopy (EC-OCWLS). EC-OWLS combines evanescent-field optical sensing with electrochemical control of surface adsorption processes.

This technique, firstly presented in 2012, is based on grating-assisted coupling of light into an optical waveguide layer [71]. The angle of the incident light beam is then varied, exciting both guided transverse electric (TE) and transverse magnetic (TM) modes. As the optical mode penetrates into the supporting solution for a distance of about 200 nm beyond the surface, the in-coupling angle of the incident light is sensitive to the refractive index and the thickness of the adsorbed film on the surface. A layer of indium tin oxide (ITO) is deposited on top of the waveguide and serves as both a high-refractive-index waveguide and conductive electrode, being completely compatible with the constraints of optical sensing (Fig. 2.13).

EC-OCWLS can further be exploited to calculate the refractive index of the layer deposited on the ITO surface. This calculation is performed by measuring both TE and TM modes, as detailed in [72]. Alternatively, EC-OWLS has been reported to be able to measure adsorbed mass down to 0.5% of an average protein layer, showing its capabilities for studying protein adsorption kinetics [73].

### 2.4.4 *Electro-Photonic Silicon Biosensing*

It has become clear that with the introduction of the personalised medicine (PM) [74], portable, compact and reliable sensing devices will be required in the near future. For example, particular diseases, such as cancer, will require detection of biomarker profiles to personalise diagnosis and treatment. The SOI platform is, therefore, conveniently positioned to address this challenge presented by PM, as its CMOS com-

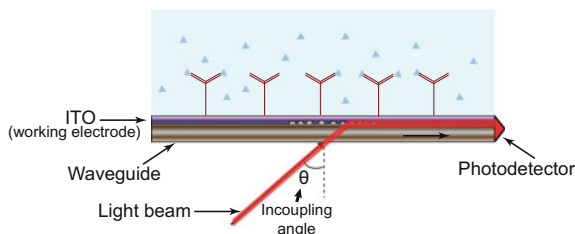
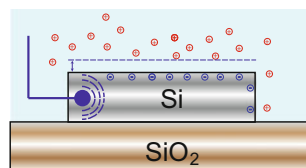


**Fig. 2.13** Electrochemical Optical Waveguide Lightmode Spectroscopy (EC-OCWLS). Light coupled into the waveguide through a grating coupler changes its in-coupling angle when the refractive index on top of the sensor surface is modified

**Fig. 2.14** Electro-photonic silicon biosensing. Electrochemical control to the surface of a SOI sensor is provided, allowing optical evanescent field sensing



patibility allows the development of such cheap and precise point-of-care devices which will be able to monitor multiple biomarkers in parallel.

Nevertheless, this platform can also be complemented by performing parallel sensing in a complementary domain, here the electrochemical (Fig. 2.14). In this way, information about the electrochemical activity of immobilised molecules, and deeper insight into molecular and (bio)molecular processes, can be provided in addition to that supplied by the optical domain. This novel sensing system, namely electrochemical-photonic silicon biosensing, is the object of study of this thesis.

To successfully combine both the electrochemical and optical domains, an electrochemically compatible layer has to be integrated within the SOI platform. For instance, an electrochemically and optically compatible layer could be deposited on the silicon layer of the SOI substrate or the electrical properties of the SOI substrate itself can be modified. The viability of both approaches is studied in Sect. 4.1.

This bi-domain system would take advantage of the SOI sensor platform (i.e. freedom to choose the optical structure for sensing, tailoring of light-matter interaction and read-out integration) while simultaneously conducting (and monitoring) electrochemical reactions occurring on the silicon surface. This not only provides insight into electrochemical processes but can also be exploited for chemical modification of the photonic sensors.

## 2.5 Self-assembled Monolayers

A critical component of all label-free technologies is the need to immobilise capture molecules onto the sensor surface using a process that must preserve the high affinity and selectivity of the capture molecule against the target biomarker.

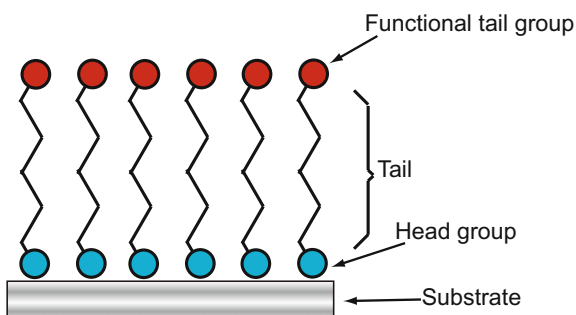
A number of different methods can be employed to anchor capture molecules to the surface of a label-free transducer. The most basic approach is to allow the capture molecules to bind non-specifically to the transducer surface through electrostatic and/or hydrophobic interactions. While simple, this approach is rarely used due to the following reasons. On the one hand, it leads to non-specific interactions on the surface, as the surface itself is not selective to any particular chemistry. Covalent attachment is also desired rather than non-specific interactions in order to immobilise the molecules on the surface. Furthermore, non-specific interactions do not allow to control the surface density or, when possible, the orientation of immobilised molecules. This is very important in biosensing as the need to optimise the bioassay

conditions for the detection of molecules. Controlling the surface density allows to prevent steric hindrance, effect which can limit the performance of biosensors [75]. Finally, when proteins are used as capture molecules, their stability is affected when they are brought into contact with inorganic material, as they undergo a change in their structure (generally unfolding) with the loss of activity [76].

A more controlled approach to immobilisation is to pre-functionalise the surface in order to control the surface chemistry. This functionalisation, which can be patterned in different ways [77], introduces chemical functional groups to the surface of the transducer which can further link to other molecules through covalent chemical bonding.

The most widely utilised method of surface functionalisation is based on Self-Assembled Monolayers (SAMs). SAMs have received significant interest due to their ability to modify and control the chemistry and properties of planar surfaces, including semiconductors and metals, and curved surfaces, such as nanoparticles, as they form a well-ordered and stable thin film. SAMs are molecular assemblies spontaneously formed on surfaces by adsorption of a surfactant on a solid surface. Note that adsorption refers to the adhesion of atoms, ions, or molecules from a gas, liquid, or dissolved solid to a surface, while absorption relates a physical or a process in which atoms, molecules or ions enter some bulk phase. In contrast with ordinary surfactant monolayers, the molecules which form the SAM typically possess a chemical moiety (the head group as depicted in Fig. 2.15), that has a strong affinity for the substrate and thus tethers the molecule stably to the surface to expose the tail group (which acts as a physical barrier and provides a well-defined thickness). These functional tail groups are typically chemically functional, for example thiols (-SH), hydroxyls (-OH) and amines (-NH<sub>2</sub>), allowing the covalent coupling of receptor molecules, as required for the design of label-free biosensor. In addition to chemical functionality for molecular immobilisation, SAMs can also provide further control of surface properties including chemical resistance, biocompatibility, wetting and adhesion [78]. The most widely investigated SAMs are those based on monolayers of alkanethiols on gold substrates [79].

**Fig. 2.15** Schematic of a SAM on a substrate. The “head group” is chemically absorbed onto the substrate, followed by a slow rearrangement of “tail groups” driven by intermolecular interactions between the organic tail region



### 2.5.1 Formation of Self-assembled Monolayers

SAMs are created by the chemisorption of head groups onto the substrate from either liquid or vapour phase, followed by a slow rearrangement of “tail groups”. The formation process is driven by the minimisation of energy in the formation of the layer, as adsorption lowers the surface free-energy of the system [78]. The main energies involved in the assembly of the monolayer are four: the energy of adsorption of the headgroup to the surface ( $\Delta E_{ads}$ ), the energy related to the corrugation of the surface ( $\Delta E_c$ ), the Van de Waals energies between the backbones ( $\Delta E_v$ ) and the energy associated with the conformational isomers of adjacent groups along the backbone (gauche conformation in the case of alkane chains) ( $\Delta E_g$ ). These energies are depicted in Fig. 2.16.

A key aspect for the quality of the SAM is the surface topography of the substrate. Surface roughness on the scale of the molecule will have a direct impact on the SAM quality, as the integrity of the SAM is inversely proportional to the roughness dimensions. Indeed, the quality of the SAM is more associated to the amount of grains in the substrate than to the amount of adsorbed molecules which construct the SAM [78]. However, if optimised, it has been reported that the roughness of the SAM can be employed to reduce non-specific adsorption in microfluidic biosensors [80].

### 2.5.2 Assembly of Silane SAMs on Silicon

Alkoxysilanes are some of the most common chemistries employed for the assembly of SAMs on both silicon and glass substrates through a process known as silanisation. Silanisation requires substrates to contain hydroxyl groups on the surface in order to form a covalent Si-O-Si bond between the surface and the alkoxysilane [78]. An example for the formation of a 3-Mercaptopropyltrimethoxysilane (MPTS) layer on silicon is shown in Fig. 2.17, which provides a thiol modification to the silicon substrate.

Although organosilane layers are typically disordered, they exhibit high stability once assembled, and show greater robustness to desorption than alkanethiol monolayer-

**Fig. 2.16** Principal energies associated with formation of SAMs. The whole formation process is driven by the minimisation of energy in the formation of the layer

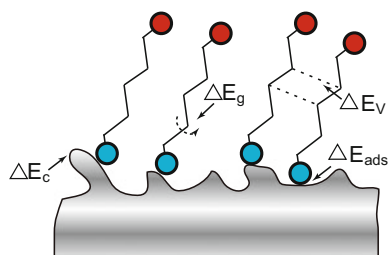
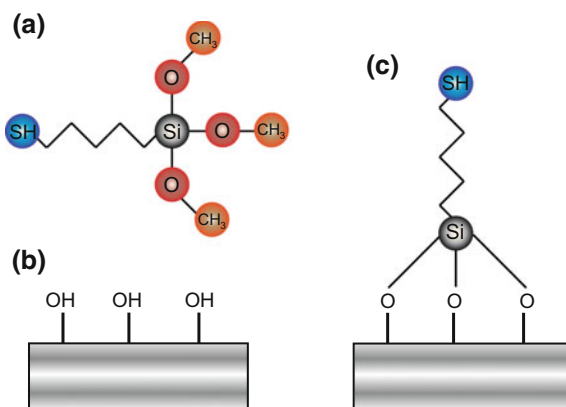




**Fig. 2.17** Formation of a 3-Mercaptopropyltrimethoxysilane (MPTS) layer on silicon. **a** 3-Mercaptopropyltrimethoxysilane molecule requires hydroxyl groups on the surface **b** to form a covalent Si-O-Si bond to the surface **c**



ers formed on gold [81]. Improvements to the order and reproducibility of organosilane layers requires minimisation of water content (both in the solution and on the surface). Excess presence of water molecules in the solution promotes the formation of polysiloxanes in the solution-phase and the assembly of multilayers on the surface [82], which decreases the quality of the layer.

## 2.6 Summary

This chapter has introduced the main motivation for the development of label-free biosensors, as the need of biofunctionalisation such label-free transducers for the detection of biomolecules in their native conformation. The most widespread label-free detection strategies in both electrical and photonic domains have been highlighted, providing a summary of their sensing principles and main applications. More specifically, photonic waveguide-based detection strategies, and in particular ring resonator biosensors, have been the focus. The evanescence field sensing principle of such resonators has been extensively presented, as the devices here developed base their optical sensing mechanism in this effect. Subsequently, the chapter has followed with an introduction to bi-domain sensing techniques. It has been shown how the added value of these label-free dual-mode systems will help to understand complex molecular and biomolecular processes. The chapter follows introducing the highly novel dual-mode electrochemical-photonic sensing technique developed in this thesis, which is capable of, for instance, exploiting chemical modification of the photonic sensors, monitoring in situ electrochemical reactions occurring on the silicon surface or enzyme activity in parallel with substrate binding. Finally, a summary of the most common functionalisation techniques for silicon surfaces based on SAMs is given.

## References

1. M.A. Cooper, *Label-Free Biosensors Techniques and Applications* (Cambridge University Press, 2009)
2. R.M. Lequin, Enzyme immunoassay (EIA)/ enzyme-linked immunosorbent assay (ELISA). *Clin. Chem.* **51**(12), 2415–2418 (2005)
3. T.G. Campbell, S.C. Howes, D.R. Fournier, L. Song, T. Piech, P.P. Patel, L. Chang, A.J. Rivnak, E.P. Ferrell, J.D. Randall, G.K. Provuncher, D.R. Walt, D.M. Rissin, C.W. Kan, D.C. Duffy, Single-molecule enzyme-linked immunosorbent assay detects serum proteins at subfemtomolar concentrations. *Nat. Biotechnol.* **28**, 595–599 (2010)
4. S. Ray, G. Mehta, S. Srivastava, Label-free detection techniques for protein microarrays: prospects, merits and challenges. *Proteomics* **1002**(10), 731–748 (2009)
5. J. Homola, S. Yee, G. Gauglitz, Surface plasmon resonance sensors: review. *Sens. Actuators* **54**(54), 3–15 (1999)
6. GE Healthcare. Biacore, 2006, <https://www.biacore.com/lifesciences/index.html>
7. M. Alvarez, M. Carmen, Estevez, L.M. Lechuga, Integrated optical devices for lab-on-a-chip biosensing applications. *Laser Photon. Rev.* **6**(4), 463487 (2012)
8. J.M. Rodriguez-Frade, M. Mellado, J. Trevio, A. Calle, and L.M. Lechuga, Determination of human growth hormone in human serum samples by surface plasmon resonance immunoassay. *Talanta* **78**(3), 1011–1016 (2009)
9. J. Homola, Surface plasmon resonance sensors for detection of chemical and biological species. *Chem. Rev.* **108**(2), 462–493 (2008)
10. B.T. Cunningham, L. Laing, Microplate-based, label-free detection of biomolecular interactions: applications in proteomics. *Expert Rev. Proteomics* **3**(3), 271–281 (2006)
11. R. Puchades, M.-J. Bauls, N. Maquieira, Chemical surface modifications for the development of silicon-based label-free integrated optical (io) biosensors: a review. *Analytica Chimica Acta* **777**, 1–16 (2013)
12. J.C. Ramirez A. Fernandez Gavela, D. Grajales Garca and L. M. Lechuga. Last advances in silicon-based optical biosensors. *Sensors* **16**(3):285–300, 2016
13. J.C. Hoogvliet, M. Dijkstra, B. Kamp, W.P. van Bennekom. Development of an electrochemical immunosensor for direct detection of interferon-gamma at the attomolar level. *Anal. Chem.* **73**(3), 901–907 (2001)
14. Y. Cui, W.U. Wang, G.F. Zheng, F. Patolsky, C.M. Lieber, Multiplexed electrical detection of cancer markers with nanowire sensor arrays. *Nat. Biotechnol.* **23**(10), 1294–1301 (2005)
15. Florian Reuter Martin Nirschl, Janos Vrs, Review of transducer principles for label-free biomolecular interaction analysis. *Biosensors* **1**, 70–92 (2011)
16. A.P.F. Turner, Biosensors: sense and sensibility. *Chem. Soc. Rev.* **42**, 3184–3196 (2013)
17. X. Luo, J. Davis, Electrical biosensors and the label free detection of protein disease biomarkers. *Chem. Soc. Rev.*, 5944–5962 (2013)
18. S. Liu, X. Guo, Carbon nanomaterials field-effect-transistor-based biosensors. *Npg Asia Mater.*, 121–131 (2012)
19. J.H. Niazi Y. Gurbuz B.S. Youn, J.W. Park, S.S. Kallempudi, M.B. Gu, Rapid and sensitive detection of nampt (pbeff/visfatin) in human serum using an ssdna aptamer-based capacitive biosensor. *Biosens. Bioelectron.*, 233–238 (2012)
20. W. Lorenz, K.D. Schulze, Zur anwendung der transformationsimpedanzspektrometrie. *J. Electroanal. Chem. Interfacial Electrochem.* (1975)
21. P. Bergveld, The development and application of fet-based biosensors. *Biosensors*, 15–33 (1986)
22. L.C. Clark, C. Lyons, Electrode systems for continuous monitoring in cardiovascular surgery. *Ann. New York Acad. Sci.* **102**(1), 29–45 (1962)
23. J. Wu, L. Yin, Platinum nanoparticle modified polyaniline-functionalized boron nitride nanotubes for amperometric glucose enzyme biosensor. *ACS Appl. Mater. Interfaces* **3**(11), 4354–4362 (2011)

24. Q. Xie, D. Yang, H. Xiao, Y. Fu, Y. Tan, C. Chen, S. Yao, Recent advances in electrochemical glucose biosensors: a review. *RSC Adv.* **3**, 4473–4491 (2013)
25. L. G. Bachas K. M. L. May, A. Vogt, K. W. Anderson. Vascular endothelial growth factor as a biomarker for the early detection of cancer using a whole cell-based biosensor. *Anal. Bioanal. Chem.*, 1010–1116 (2005)
26. B. Li, K.I. Chena, Y. Chena, The development and application of fet-based silicon nanowire field-effect transistor-based biosensors for biomedical diagnosis and cellular recording investigation. *Nano Today*, 131–154 (2011)
27. J.Y. Huang, M.H. Yun, X.L. Luo, I. Lee, X.Y.T. Cui, Ultrasensitive protein detection using an aptamer-functionalized single polyaniline nanowire. *Chem. Commun.* **47**(12), 6368–6370 (2011)
28. X.L. Luo, M.Y. Xu, J.J. Davis, The label free picomolar detection of insulin in blood serum. *Biosens. Bioelectron.* **39**(1), 21–25 (2013)
29. H. Rahmani, B. Rezaei, N. Majidi, T. Khayamian, Electrochemical impedimetric immunosensor for insulin like growth factor-1 using specific monoclonal antibody-nanogold modified electrode. *Biosens. Bioelectron.* **26**(5), 2130–2134 (2011)
30. A. Abulrob, A.C. Tavares, R. Elshafey, C. Tlili, M. Zourob, Label-free impedimetric immunosensor for ultrasensitive detection of cancer marker murine double minute 2 in brain tissue. *Biosens. Bioelectron.* **39**(1), 220–225 (2013)
31. N. Zine, G. Gabriel, A. Guimera, F. J. del Campo, R. Villa, A. H. Eisenberg, M. Mrksich, A. Errachid, J. Aguilo, E. Prats-Alfonso, X. Sisquella, F. Albericio, Cancer prognostics by direct detection of p53-antibodies on gold surfaces by impedance measurements. *Small* **8**(1), 2106–2115 (2012)
32. B.R. Li, K.I. Chen, Y.T. Chen, Silicon nanowire field-effect transistor-based biosensors for biomedical diagnosis and cellular recording investigation. *Nano today* **6**(2), 131–154 (2011)
33. A.O. Aluoch, O.A. Sadik, A.L. Zhou, Status of biomolecular recognition using electrochemical techniques. *Biosens. Bioelectron.* **24**(9), 2749–2765 (2009)
34. W. Bogaerts, R. Baets, P. Dumon, V. Wiaux, S. Beckx, D. Taillaert, B. Luyssaert, J. Van Campenhout, P. Bienstman, D. Van Thourhout, Nanophotonic waveguides in silicon-on-insulator fabricated with cmos technology. *J. Lightwave Technol.* **23**(1), 401–412 (2005)
35. D.J. Griffiths, *Introduction to Electrodynamics*, 3rd edn. (Prentice-Hall International Inc., NJ 07458, 1999)
36. K. Okamoto. *Fundamentals of Optical Waveguides*(Elsevier, 2006)
37. R.G. Heideman, P.V. Lambeck, Remote opto-chemical sensing with extreme sensitivity: design, fabrication and performance of a pigtailed integrated optical phase-modulated machzehnder interferometer system. *Sens. Actuators B: Chem.* **61**(13), 100 – 127 (1999), <http://www.sciencedirect.com/science/article/pii/S092540059900283X>
38. C. Domnguez, K.E. Zinoviev, A.B. Gonzalez-Guerrero, L.M. Lechuga, Integrated bimodal waveguide interferometric biosensor for label-free analysis. *J. Lightwave Technol.* **13**(29) (2011)
39. Y.A. Vlasov, S. Assefa, C. Kang, C.T. Phare, S.M. Weiss, Photonic crystal slab sensor with enhanced surface area. *Opt. Express* **18**(26), 27930–27937 (2010a)
40. S. Lee, S. Chan, Eom, J. Soo Chang, C. Huh, G. Yong Sung, J. H. Shin, Label-free optical biosensing using a horizontal air-slot sinx microdisk resonator. *Opt. Express* **18**(20), 20638–20644 (2010)
41. M.G. Scullion, T.F. Krauss, A. Di Falco, Slotted photonic crystals for biosensing applications. *Proc. SPIE* **8425**, 842507–842508 (2012)
42. C.A. Barrios, K.B. Gylfason, B. Sanchez, A. Griol, H. Sohlstrom, M. Holgado, R. Casquel, Slot-waveguide biochemical sensor. *Opt. Lett.* **32**(21), 3080–3082 (2007)
43. K. De Vos, I. Bartolozzi, E. Schacht, P. Bienstman, R. Baets, Silicon-on-insulator microring resonator for sensitive and label-free biosensing. *Opt. Express* **15**(12), 7610–7615 (2007)
44. K. Woo, K.J. Sheng Kee, Y. Shin, K. Han, Y. Yoon, G. Qiang, L.Q. Liu, X. Tu, M. Kyoung Park, Highly sensitive machzehnder interferometer biosensor based on silicon nitride slot waveguide. *Sens. Actuators B: Chem.* **188**, 681–688 (2013)

45. A. B. Gonzalez-Guerrero J. Osmond K. Zinoviev B. Sepulveda C. Dominguez S. Dante, D. Duval, L. M. Lechuga, Towards a complete lab-on-chip system using integrated mach-zehnder interferometers. *Opt Pure Appl.* **45**:87–95, 2012
46. S. Xiao, N. Mortensen, Highly dispersive photonic band-gap-edge optofluidic biosensors. *J. Eur. Opt. Soc. Rapid publications* **1**(0) (2006)
47. C. Smith, M.W. Lee, S. Tomljenovic-Hanic, C. Grillet, C. Monat, L. O’Faolain, C. Karnutsch, T.F. Krauss, R.C. McPhedran, U. Bog, L. Cameron, B.J. Eggleton, High-q microfluidic cavities in silicon-based two-dimensional photonic crystal structures. *Opt. Lett.* **33**(19), 2206–2208 (2008)
48. T.-Y. Chang, M. Huang, A.A. Yanik, H. Altug, Sub-wavelength nanofluidics in photonic crystal sensors. *Opt. Express* **17**(26), 24224–24233 (2009)
49. E. Hallynck, P. Bienstman, Photonic crystal biosensor based on angular spectrumanalysis. **18**(17), 1816418170 (2010)
50. M.R. Lee, P.M. Fauchet, Two-dimensional silicon photonic crystal based biosensing platform for protein detection. *Opt. Express* **15**(8), 4530–4535 (2007)
51. M.A. Dünder, R. Nötzel, M.J. van der Hoek, S. He, B. Wang, T. Siahaan, R.W. van der Heijden, Photonic crystal cavity on optical fiber facet for refractive index sensing. *Opt. Lett.* **37**(5), 833–835 (2012)
52. K.L. Watkin, L.L. Chan, S.L. Gosangari, B.T. Cunningham, A label-free photonic crystal biosensor imaging method for detection of cancer cell cytotoxicity and proliferation. *Apoptosis* **12**(6), 1061–1068 (2007)
53. D. Stellinga, M.G. Scullion, G.J.O. Evans, G.J. Triggs, M. Fischer, T.F. Krauss, Spatial resolution and refractive index contrast of resonant photonic crystal surfaces for biosensing. *IEEE Photon. J.* **7**(3), 1–10 (2015)
54. W.C. Lai, C.Y. Lin, Y. Zou, S. Chakravarty, R.T. Chen, Methods to array photonic crystal microcavities for high throughput high sensitivity biosensing on a silicon-chip based platform. *Lab Chip* **12**, 2309–2312 (2012)
55. Genalyte. Genalyte, 2009, <http://www.genalyte.com/>
56. W. Bogaerts, P. De Heyn, T. Van Vaerenbergh, K. De Vos, S. Kumar, T. Selvaraja, P. Claes, P.Bienstman Dumon, D. Van Thourhout, R. Baets, Silicon microring resonators. *Laser Photon. Rev.* **6**(1), 47–73 (2012)
57. K. De Vos, Label-free silicon photonics biosensor platform with microring resonators. PhD thesis, University of Ghent, 2010
58. T. Klaes, Advanced silicon photonic ring resonator label-free biosensors. *University of Ghent*, 2012
59. A. Densmore, D.X. Xu, P. Waldron, S. Janz, P. Cheben, J. Lapointe, A. Delage, B. Lamontagne, J.H. Schmid, E. Post, A silicon-on-insulator photonic wire based evanescent field sensor. *IEEE Photon. Technol. Lett.* **18**, 2520–2522 (2006)
60. J.C. Aldridge, T.A. Desai, J. Hryniewicz, N. Chbouki, B.E. Little, O. King V. Van, S. Chu, D. Gill, M. Anthes-Washburn, M.S. Unlu, A. Yalcin, K.C. Papat, B.B. Goldberg, Optical sensing of biomolecules using microring resonators. *IEEE J. Sel. Top. Quant. Electron.* **12**(1), 148–155 (2006)
61. B. Spaugh, F. Tybor, W.G. Gunn, M. Hochberg, T. Baehr-Jones, R.C. Bailey, M. Iqbal, M.A. Gleeson, L.C. Gunn, Label-free biosensor arrays based on silicon ring resonators and high-speed optical scanning instrumentation. *IEEE J. Sel. Topics Quantum Electron.* **16**(3), 654–661 (2010)
62. S. Choi, I. Jang, J.S. Choi, H.I. Jung, H.J. Lee, J.H. Lee, Asymmetric split-ring resonator-based biosensor for detection of label-free stress biomarkers. *Appl. Phys. Lett.* **103**(5) (2013)
63. A. Kazmierczak, F. Dortu, M.J. Banuls, Polo A. Maquieira Catala, G.M. Kresbach, H. Sohlstrom, T. Moh, L. Vivien, J. Popplewell, G. Ronan, C.A. Barrios, G. Stemmea, C.F. Carlborg, K.B. Gylfason, W. van der Wijngaarta, A packaged optical slot-waveguide ring resonator sensor array for multiplex label-free assays in labs-on-chips. *Lab Chip* **10**(5), 281–290 (2010)

64. P. Taranekar, R.R. Ponnappati, W. Knoll, A. Baba, R.C. Advincula, Electrochemical surface plasmon resonance (ec-spr) and waveguide enhanced glucose biosensing with n-alkylaminated polypyrrole/glucose oxidase multilayers. *ACS Appl. Mater. Interfaces* **2**(8), 2347–2354 (2010)
65. Michael Rodahl, Bengt Kasemo, A simple setup to simultaneously measure the resonant frequency and the absolute dissipation factor of a quartz crystal microbalance. *Rev. Sci. Instrum.* **67**(9), 3238–3241 (1996)
66. Yong Chen, Hai Ming, Review of surface plasmon resonance and localized surface plasmon resonance sensor. *Photon. Sensors* **2**(1), 37–49 (2012)
67. Long range surface plasmon resonance for increased sensitivity in living cell biosensing through greater probing depth. *Sens. Actuators B: Chem.* **174**, 94–101 (2012)
68. A. Reisinger, Characteristics of optical guided modes in lossy waveguides. *Appl. Opt.* **12**(5), 1015–1025 (1973)
69. S. Ehsan, Salamifar and Rebecca Y. Lai. Application of electrochemical surface plasmon resonance spectroscopy for characterization of electrochemical DNA sensors. *Colloids Surfaces B: Biointerfaces* **122**, 835–839 (2014)
70. L. Coche-Guérentee, S. Armand, P. Labbé, A. Bouchet-Spinelli, B. Reuillard, S. Fort, Oligosaccharide biosensor for direct monitoring of enzymatic activities using qcm-d. *Biosens. Bioelectron.* **49**, 290–296 (2013)
71. J.A. Hubbell J.P. Bearinger, J. Vrs, M. Textor, Electrochemical optical waveguide lightmode spectroscopy (ec-owls): A pilot study using evanescent-field optical sensing under voltage control to monitor polycationic polymer adsorption onto indium tin oxide (ito)-coated waveguide chips. *Biotechnol. Bioeng.* **82**(4), 465–473 (2003)
72. J.J. Ramsden, Review of new experimental techniques for investigating random sequential adsorption. *J. Stat. Phys.* **73**(5), 853–877 (1993a)
73. A. Marti, M. Textor, P. Tengvall, J.J. Ramsden, R. Kurrat, B. Wlivaara, N.D. Spencer, Plasma protein adsorption on titanium: comparative in situ studies using optical waveguide lightmode spectroscopy and ellipsometry. *Colloids Surfaces B: Biointerfaces* **11**(4), 187–201 (1998)
74. A.D. Weston, L. Hood, Systems biology, proteomics, and the future of health care: toward predictive, preventative, and personalized medicine. *J. Proteome Res.* **2**(3), 179–196 (2004)
75. A.D. Edwards, Steric hindrance effects on surface reactions: applications to biacore. *J. Math. Biol.* **55**(4), 517–539 (2007)
76. R.A. Edwards, R.E. Huber, Surface denaturation of proteins: the thermal inactivation of beta-galactosidase (escherichia coli) on wall-liquid surfaces. *Biochem Cell Biol.* **70**(1), 63–69 (1992)
77. P. Colpo, A. Ruiz, L. Ceriotti, F. Rossi, *Surface Functionalization for Protein and Cell Patterning* (Springer, Berlin, 2010), pp. 109–130
78. A. Ulman, Formation and structure of self-assembled monolayers. *Chem. Rev.* **96**, 1533–1554 (1996)
79. W.C. Bigelow, D.L. Pickett, W.A. Zisman, Oleophobic monolayers. *J. Colloid Sci.* **1**(6), 513–538 (1946)
80. Seokheun Choi, Junseok Chae, Methods of reducing non-specific adsorption in microfluidic biosensors. *J. Micromech. Microeng.* **20**(7), 075015 (2010)
81. Y. Tai Tao, S.R. Wasserman, G.M. Whitesides, Structure and reactivity of alkylsiloxane monolayers formed by reaction of alkyltrichlorosilanes on silicon substrates. *Langmuir* **5**(4), 1074–1087 (1989)
82. T. Okubo, Y. Yamaguchi, M. Hu, S. Noda, Hiroshi Komiyama, Structure and morphology of self-assembled 3-mercaptopropyltrimethoxysilane layers on silicon oxide. *Appl. Surface Sci.* **181**(34), 307–316 (2001)

Dual-Mode Electro-photonics Silicon Biosensors

José, J.-C.

2017, XV, 149 p. 105 illus., 89 illus. in color., Hardcover

ISBN: 978-3-319-60500-5